ELSEVIER

Applied Catalysis A: General 226 (2002) 49–61

APPLIED CATALYSIS A: GENERAL

www.elsevier.com/locate/apcata

Vapor phase nitration of toluene using dilute nitric acid and molecular modeling studies over beta zeolite

Sharda P. Dagade, Suresh B. Waghmode, Vijay S. Kadam, Mohan K. Dongare*

Catalysis Division, National Chemical Laboratory, Pune 411 008, India

Received 9 April 2001; received in revised form 25 June 2001; accepted 3 September 2001

Abstract

The regio-selective nitration of toluene to *para*-nitrotoluene with dilute HNO_3 has been studied over catalyst beta zeolite. The effect of reaction temperature, concentration of HNO_3 and molar ratio of toluene to HNO_3 is reported. The maximum conversion of 55% (toluene to HNO_3 ratio, 1.7:1), selectivity to *para*-nitrotoluene of 70%, and catalyst life of 75 h (weight hourly space velocity (WHSV) = 0.2) were obtained using 20% nitric acid at temperature of 120 °C. The catalyst deactivated faster when the concentration of acid and the temperature of reaction and WHSV was increased. The physicochemical characterization of the deactivated catalyst showed the structural stability of beta zeolite under the reaction conditions, but the *para*-nitrotoluene, and other oxidation products 4-nitrobenzoic acid, benzaldehyde, benzoic acid and anthraquinone were found deposited on the catalyst surface. Even then, the selectivity for *para*-nitrotoluene remains nearly constant. The molecular modeling study revealed that *para*-nitrotoluene encounters the least resistance for diffusion in the beta zeolite. These observations indicate that the shape selective nitration of toluene takes place inside the zeolite pores. The catalyst with alumina binder was found to be more active than the catalyst without binder because of higher acidity. The deactivated catalyst can almost be regenerated by washing the catalyst with organic solvents.

Keywords: Toluene nitration; Deactivation; Shape-selectivity; Modeling; Diffusion; Beta

1. Introduction

Nitrotoluenes are important intermediates in the chemical industry, are industrially produced by liquid phase nitration of toluene using a mixture of nitric and sulfuric acid as a nitrating agent [1]. The typical product distribution of *ortho*-, *meta*- and *para*-isomers in the conventional nitration is about 58:4:38, whereas the thermodynamic equilibrium concentration is 29:33:38, respectively [2]. The *para*-isomer has better commercial value as the pharmaceutical intermediate and is sold at about three times the cost of the *ortho*-isomer [3]. A large quantity of dilute sulfuric acid is generated as waste in the conventional process and its disposal or recycle is very expensive; this makes the toluene nitration one of the most environmentally harmful processes. The replacement of sulfuric acid with solid acid catalyst with high selectivity for *para*-isomer would be an attractive environmentally benign route for the production of nitrotoluenes.

Several solid acid catalysts have been investigated for the liquid and vapor phase nitration process. McKee and Wilhelm [4] used silica gel as a solid acid catalyst for the vapor phase nitration of benzene and toluene. Other solid acid catalysts studied for nitration are sulfonated polyorganosiloxanes [5,6],

* Correspondence author. Tel.: +91-20-5893300x2044; fax: +91-20-589-3761x3355.
E-mail address: dongare@cata.ncl.res.in (M.K. Dongare).

0926-860X/02/$ – see front matter
PII: S0926-860X(01)00882-1

acidic resins [7], modified clays [8], zeolites [9–11], sulfated zirconia [12], supported sulfuric acids [13], and supported sulfonic acid [14].

Among acidic zeolite catalysts such as H-mordenite, H-beta, H-ZSM-5 and H-Y, zeolite H-beta has shown higher conversion and remarkable selectivity for *para*-isomer in vapor phase nitration of toluene. Choudary et al. [15] carried out the nitration of toluene in liquid phase employing nitric acid of 60–90% concentration over solid acid catalyst and by azeotropic removal of water. Beta zeolite proved to be the best catalyst among the zeolites, in terms of space–time yield (STY), *para*-selectivity and consistent activity and selectivity even after five cycles without dealumination of the catalyst. Prins and co-workers [16] investigated the nitration of toluene in the gas phase at 158 °C with 65% nitric acid over zeolite catalyst; among the catalysts studied, zeolite H-beta showed promising results. The activity and selectivity decreased over a period of about 5 h on stream, due to pore filling/blockage by strongly adsorbed products/byproducts. Nitration of toluene using H-beta zeolite catalyst to replace the sulfuric acid in the conventional process could not be commercialized because of deactivation of catalyst, leading to low space time yields.

Smith et al. [17] have investigated deactivation and shape-selectivity effects in toluene nitration in vapor phase with NO_2 as nitrating agent, as well as in liquid phase using *n*-propyl nitrate over zeolite, MCM-41 and sulfated zirconia catalysts. Almost all the catalysts exhibited deactivation over a period of about 5 h on stream due to pore filling/blockage by strongly adsorbed products and byproducts.

However, the deactivated catalysts and the byproducts formed after deactivating the catalyst were not fully enough characterized to understand the deactivation process. The concentrated nitric acid (65–70 wt.%) and higher temperature (160 °C) used in the earlier studies led to the oxidative side reactions, resulting in faster deactivation of the catalyst. We have studied the vapor phase nitration of toluene using beta zeolite catalyst with dilute nitric acid of different concentrations at various temperatures and the deactivated catalyst was analyzed using various analytical techniques to understand the deactivation process. We have also carried out molecular modeling and fitting studies for nitration of toluene over beta and MFI zeolites to highlight that this simple theoretical approach is suitable to answer the fundamentally important question of the nature of interaction of the guest molecule with zeolite lattice.

2. Experimental

2.1. Catalyst testing and characterization

Commercially available H-beta zeolite (Si/Al = 30) in the powder form (non-formulated) and in the extrudate form (formulated, Si/Al = 30, zeolite/alumina binder = 80:20) were procured from United Catalyst India Ltd. The non-formulated H-beta catalyst was compacted in the form of pellets and further granulated to 20 mesh size for use in nitration reactions. Vapor phase nitration experiments were performed in a fixed-bed continuous down flow glass reactor at atmospheric pressure. Ten grams of the catalyst was loaded in a tubular glass reactor of 15 mm diameter and 25 mm length. The upper part of the reactor was packed with inert ceramic beads as the preheating zone. Before the reaction, the catalyst sample was preheated at 450 °C for 12 h in a 10 ml/min flow of air. Then the reactions were carried out by passing aqueous dilute nitric acid and toluene using syringe pumps (Sage feed pump), in the temperature range of 120–200 °C with nitrogen as carrier gas at the rate of 10 cm^3/min. The weight hourly space velocity (WHSV) was varied from 0.1 to 1 h^{-1}.

The reaction product was collected in a receiver maintained at 5 °C. This product was extracted with diethyl ether, and the extracted product was analyzed off-line by gas chromatography (HP5890, column SPB-1, 30 m, 0.53 mm i.d.), GC/MS (SHIMADZU, column, DB-I) and FTIR (Nicolet-60, SXB). The catalyst was characterized before and after the reaction for its physical and chemical properties using various techniques such as XRD (Regaku, Miniflex), surface area (Omnisorb CX-100), TG/DTA (SETARAM TG/DTA 92), EDX (KEVEX 7000 system), FTIR (Nicolet, 60 SXB spectrometer) and AAS (Perkin-Elmer). The deactivated catalyst was washed with acetone/carbon tetrachloride and the washing was analyzed using GC, GC/MS, and GC/IR for the identification of products/byproducts deactivating the catalyst.

2.2. Methods and models

Several zeolites have been tried experimentally for this reaction. Much attention has been focused on beta due to its high activity and predominant shape-selectivity. The unique 12-member (12-M) channel system in beta has been believed to be the cause of shape-selectivity. However, medium pore zeolites with a 10-member (10-M) channel system, particularly ZSM-5 [18], have not shown considerable shape-selectivity in nitration of toluene to *para*-nitrotoluene. Although the zeolites are broadly classified as small, medium and large pore zeolites, each one of the structurally distinct 105 zeolites known to date [19], has different architecture and hence, the diffusion characteristics of molecules inside their pores cannot be generalized. The catalytic behavior of most of the zeolites arises from the catalytically active Bronsted acid sites. These active sites are located inside the intriguing pore structures. In such cases molecular modeling and graphics can provide better understanding of the active sites.

The computational studies reported here were carried out using software programs—InsightII and Discover, supplied by Molecular Simulations Inc., USA. The force field energy minimization calculations were done with the Discover program, using consistent valence force field (CVFF) of Hagler et al. [20] and the parameters were obtained from the reports of Dauber-Osguthorpe et al. [21]. The actual values used in these calculations have been listed in our earlier work [22,23]. The interaction energy of the molecule with the zeolite framework is calculated using the force field expression [20] that contains the terms corresponding to deformation of bond lengths, bond angles, torsion angles, etc. of the molecule. The non-bonding interactions of the molecule with the zeolite framework are calculated by determining the long- and short-range forces in terms of electrostatic interaction and Lennard-Jones potentials. Molecular graphics (MG) displays were obtained from InsightII molecular modeling system using Silicon Graphics workstation. Energy minimization is carried out in a sequence with steepest-descent, conjugate gradient and Newton–Raphson algorithms.

Table 1
Dimensions of different molecules in their minimum energy configuration

Molecule	Dimensions		
	a (Å)	*b* (Å)	*c* (Å)
Nitroniumion (**1**)	4.6	3.0	2.7
Toluene (**2**)	6.9	5.3	2.8
ONT (**3**)	8.0	6.9	2.9
MNT (**4**)	8.3	7.0	2.9
PNT (**5**)	8.8	5.3	2.8
DNT (**6**)	9.9	7.1	3.0

The extents of the molecule in space were calculated for the energetically favorable conformation and their sizes and shapes were analyzed. The dimensions of molecules in three-dimensional space are measured according to the procedure detailed elsewhere [24]. The three largest dimensions ($a \times b \times c$) of the nitronium ion (**1**), toluene (**2**), *ortho*-nitrotolune (**3**), *meta*-nitrotolune (**4**) *para*-nitrotolune (**5**) and dinitrotoluene (**6**) molecules in mutually perpendicular directions are given in Table 1. Qualitative structural fitting of the molecules inside the zeolites was studied by MG as well as by comparing the dimensions of the molecules with the pore diameters of the zeolites. The zeolite lattices were generated from the X-ray crystal structures reported for MFI [25] and beta [26]. Further, the chemical interaction between the zeolite host and guest molecules was studied using energy minimization calculations to understand the adsorption sites and diffusion characteristics of the molecules **1**–**6**. The simulation box contained the zeolite generated from its crystal structure and the actual dimensions of the simulation box for each zeolite are given in Table 2.

Table 2
Crystal characteristics and the dimensions of the simulation boxes for different zeolites

Zeolite	Symmetry	Unit-cell composition	*a* (Å)	*b* (Å)	*c* (Å)	Average pore diameter (Å)	Number of unit-cell in the simulation box
MFI	Orthorhombic	$(SiO_2)_{96}$	20.022	19.899	13.383	5.1 × 5.6	2 × 3 × 2
BETA	Tetragonal	$(SiO_2)_{94}$	12.660	12.660	26.406	7.6 × 6.4	6 × 2 × 1

The size of the simulation boxes are chosen in such a way that the symmetry along the channel direction is taken care of and the box is just large enough in the other two directions to take care of the non-bonded interactions, whose cut-off distance was taken as 8.5 Å. The diffusion energy profiles symmetrically repeat themselves in each unit-cell, indicating the validity of the simulation box size, potential parameters and energy minimization calculation procedures.

The calculations were performed following the well established forced diffusion procedure. This procedure has been widely used to study the diffusion of methanol [27], toluene nitration [15], aromatic hydrocarbons [28], isomers of alkylated naphthalene [29], *n*-butane and isobutane [30], isomers of isobutylethylbenzene [22,23,31–33], isomers of acylated 2-methoxynaphthalene [34], acylated 4-hydroxyphenol [35], isomers of butene [36,37] and isomers of xylenes [23]. Here, we investigated the shape-selective production of **5** over two zeolites. The sorbate molecule was forced to diffuse in regular steps of 0.2 Å along the diffusion path defined by the initial and final positions within the channel. At each point, a strong harmonic potential constrains the molecule to lie at a fixed distance from the initial position while the energetically favorable conformation and orientation of the molecule are derived by varying the internal degrees of freedom as well as non-bonding interaction of the molecule with the zeolite framework. The interaction energy at each point is calculated using Eq. (1):

$$\text{interaction energy} = E_{\text{zeolite: molecule complex}} - (E_{\text{zeolite}} + E_{\text{molecule}}) \quad (1)$$

Thus, the diffusion energy profile is a graph showing the variation of interaction energy between a single molecule and the zeolite framework as the molecule diffuses within the channel of the zeolite. The diffusion energy profiles are useful to identify the most favorable (minimum energy) and unfavorable (maximum energy) adsorption sites for the molecules inside the zeolite channels. The difference in energy between the most favorable and most unfavorable sites in the diffusion energy profile gives the diffusion energy barrier for self-diffusivity. Since our interest is to study the influence of the pore architecture and dimensions on the diffusion characteristics of the molecules, we considered a fully siliceous zeolite lattice. The influence of the presence of more molecules on the diffusivity (mutual effect) and the influence of temperature are not considered here. In view of these approximations, suitable care was taken to interpret the results.

The mean energy is the numerical average of the interaction energy of the molecules at all locations in the diffusion path. The ratio of mean energy to minimum energy (the most favorable site) is a diffusivity index parameter. If the mean energy is close to minimum energy, the situation represents the presence of several minima and the mean/minimum energy ratio will be closer to 1. On the contrary, if the mean energy is much higher than the minimum energy, the situation represents the presence of several maxima and the mean/minimum energy ratio will be closer to 0. Thus, the ratio is an indicator of the diffusivity of the molecule; the higher the value, the greater is the diffusivity.

3. Results and discussions

3.1. Reaction study

The results of toluene nitration using dilute nitric acid over beta zeolite at different temperatures are given in Table 3. The conversion of toluene to mononitrotoluene was low (4.3%) at 90 °C and attained a maximum (55%) at 120 °C and then decreased with increase in temperature. The maximum conversion of toluene at 120 °C was 55% at toluene:nitric acid ratio of 1.7:1, with a selectivity of 73% for *para*-nitrotoluene. As the temperature of the reaction is increased from 120 to 180 °C, the oxidation products, benzaldehyde, benzoic acid and 4-nitrobenzoic acids were increased from 0.31 to 1.36% (Fig. 1) and the catalyst life was decreased from 75 to 10 h. The influence of concentration of nitric acid on toluene nitration over beta zeolite is shown in Fig. 2. It is seen that, as the concentration of nitric acid was increased from 20 to 40%, the conversion of toluene decreased and the formation of oxidation products increased, leading to a decrease in catalyst life because of the deposition of oxidation products on the surface of the catalyst. From these results it is seen that, when the toluene nitration was carried out at 120 °C with 20% nitric acid over beta zeolite, the toluene conversion and selectivity for *para*-nitrotoluene was highest.

Table 3
Effect of temperature on product distribution in toluene nitration[a]

Temperature (°C)	Conversion HNO_3 (%)	Product distribution[b] (%)			Oxidation[c] products (%)	*Para*/*ortho* ratio
		ONT	MNT	PNT		
90	8.00	2.56	0.36	1.78	0	0.70
120	83.42	12.1	2.68	33.9	0.31	2.80
140	76.96	11.3	3.38	30.6	0.45	2.71
160	70.40	10.4	2.58	27.12	1.21	2.61
180	57.60	8.9	2.4	21.6	1.36	2.51

[a] Reaction conditions: toluene:nitric acid (molar ratio) = 1.7:1; HNO_3 (wt.%) = 2%; catalyst, H-beta (formulated).
[b] ONT: *ortho*-nitrotoluene; MNT: *meta*-nitrotoluene; PNT: *para*-nitrotoluene.
[c] Oxidation products: benzaldehyde; benzoic acid; 4-nitrobenzoic acid; anthaquinone.

Under these conditions, the catalyst remains active for up to 80 h, which is higher than any values reported in the literature for any catalyst [15–17]. The deactivation of the catalyst at higher temperature than 120 °C and with concentrated nitric acid higher than 20% may be attributed to the generation of nitrous oxide (NO), which oxidizes toluene to benzaldehyde and other side chain oxidation products causing the deactivation of the catalyst [38]. Nitration of toluene is an exothermic reaction, and the use of dilute nitric acid provides water vapors, which dissipates the heat of reaction so that the formation of oxidation side products is minimized. That the dilute nitric acid is cheaper than concentrated nitric acid provides an added advantage for the commercialization of the process. The increase in WHSV from 0.2 to 1 lowered the toluene conversion as well as the catalyst life (Fig. 3). It is interesting to note that, even though the catalyst is deactivated, lowering the conversion of toluene, the selectivity for *para*-isomer remains almost constant (73%). This indicates that the oxidation products are deposited on the surface, leaving only a few pores open for the shape-selective reaction inside the pores. This may be due to the orientation of toluene molecule on the catalyst surface, causing steric hindrance for the formation of other isomers of nitrotoluene.

When the reaction is carried out using non-formulated catalyst, the conversion of toluene was less (37.6%) compared to that using formulated catalyst (55%) with similar selectivity for *para*-isomer,

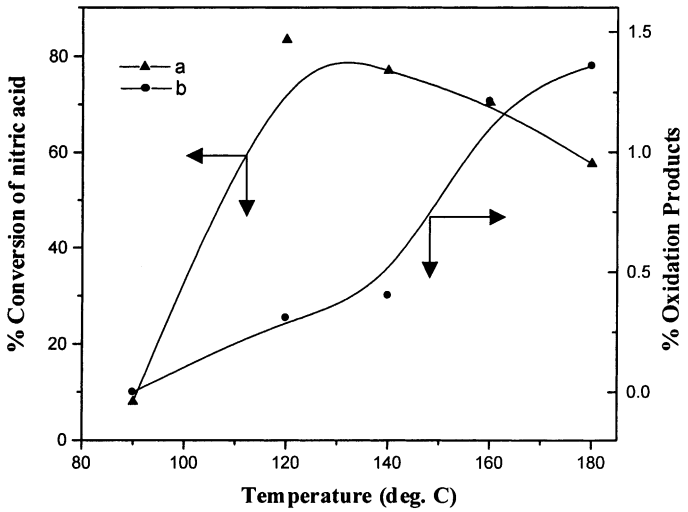

Fig. 1. Effect of temperature (°C) on formation of oxidation products over beta zeolite.

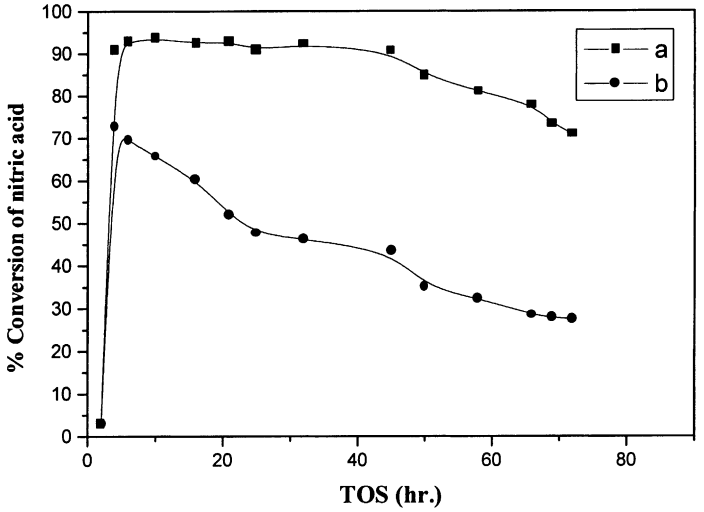

Fig. 2. Effect of dilution of nitric acid on the catalyst life: (a) performance of catalyst using 20% HNO_3 and (b) performance of catalyst using 30% HNO_3.

but the life of the catalyst was more in the case of formulated catalyst (Fig. 4). The non-formulated catalyst has mainly Bronsted acid sites which generate nitronium ions from nitric acid adsorbed on the catalyst surface, whereas the formulated catalyst has both Bronsted and Lewis acid sites because of the alumina binder, which affects the acidity of the catalyst, leading to the higher conversion compared to that with non-formulated catalyst. When the reaction was carried out over ZSM-5 (MFI) catalyst, the conversion of toluene, as well as the *para*-nitrotoluene formation, were lower as compared to the values for beta zeolite.

The deactivated catalyst, after washing with acetone and methyl ethyl ketone solvents, regains about 90% of its original activity. That indicates that the deactivation of the catalyst is partly due to fouling of

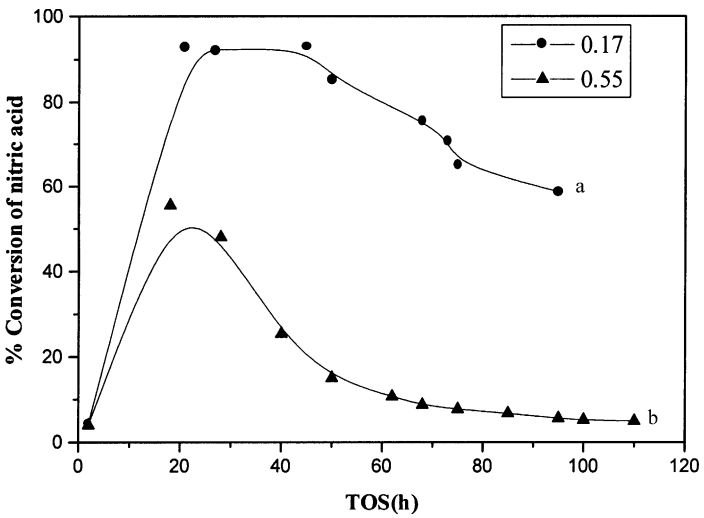

Fig. 3. Effect of WHSV on the catalyst deactivation over beta zeolite.

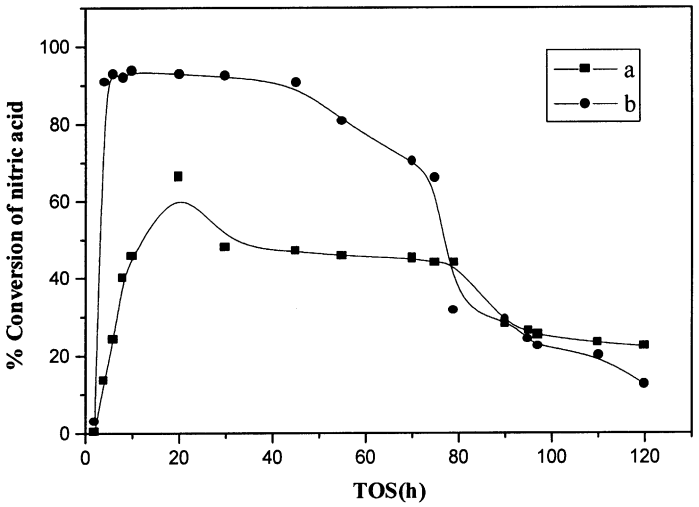

Fig. 4. Effect of binder on the activity of beta zeolite: (a) indicates beta zeolite without binder and (b) indicates beta zeolite with binder (alumina).

the catalyst surface by the deposition of the oxidation products, which are soluble in these solvents and are washed away after washing. By washing the catalyst intermittently with these solvents, one can minimize the thermal regeneration cycle of the catalyst, increasing the STY between two regeneration cycles. Such a regeneration protocol is not described in the literature.

3.2. Characterization of the deactivated catalyst

A comparison of XRD patterns of H-beta sample before and after nitration shows no loss in crystallinity, indicating the structural stability of the catalyst in acid environment of this reaction. Thermal analysis (TG/DTA/DTG) of the deactivated beta zeolite in flowing air is shown in Fig. 5. It indicates that up to 200 °C there is an endothermic weight loss of adsorbed water/toluene from the catalyst [39] and above 200–400 °C the weight loss is due to evaporation of volatile oxidation products deposited on the zeolite. The final exothermic weight loss of 12.85% below 690 °C is due to the combustion of adsorbed species, suggesting the formation of coke precursors. This shows that the adsorption of high boiler species inside the pores and on the external surface of the catalyst was responsible for the deactivation. These species may be coke precursors. In the case of non-formulated beta zeolite, the weight loss is less than that of formulated beta zeolite. The FTIR spectra of deactivated formulated zeolite showed the presence of aluminum nitrate, indicating the leaching of aluminum from binder alumina, which can also block the active sites on catalyst surface.

The FTIR spectra of chemisorbed pyridine at 100, 200, 300 and 400 °C on the fresh and reactivated beta zeolite are shown in Fig. 6a–h. The bands observed at 1636 and 1543 cm^{-1} are assigned to pyridine molecules bound to Bronsted acid sites and those at 1612, 1490, 1448 cm^{-1} are assigned to pyridine molecules bound to Lewis acid sites [40]. The IR spectra of the deactivated sample obtained at 200 °C showed the deposition of high boilers on the sample. When the pyridine was chemisorbed on a reactivated sample, the FTIR spectra revealed regeneration of both types of acid sites, which are shown in Fig. 6e–h.

The surface area which was determined according to the *t*-plot method [41] of the deactivated zeolite showed a substantial loss after nitration indicating pore filling/blockage by strongly bound byproducts (Table 4). The deactivated zeolite catalyst was washed with acetone and the washing was analyzed by GC, GC/MS, and GC/IR, results showed 4-nitrobenzoic acid, a major product, benzaldehyde, dinitrotoluene, and toluene as minor products and anthraquinone in trace quantities.

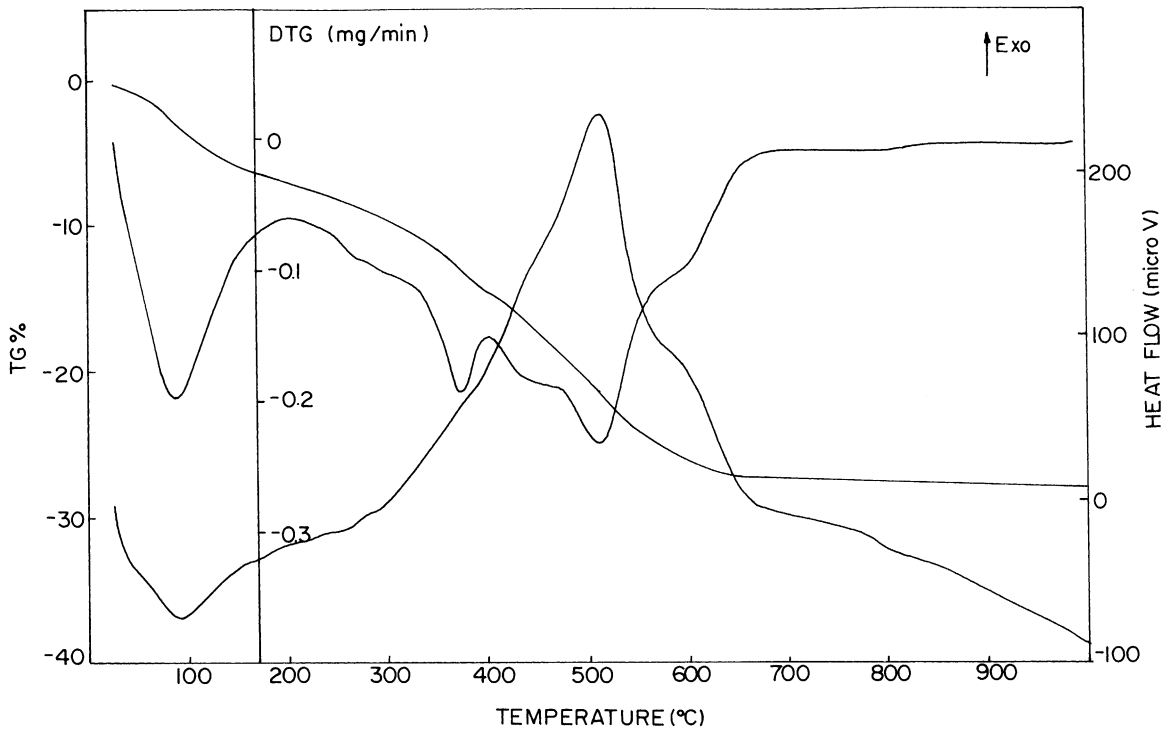

Fig. 5. Thermal analysis of deactivated beta zeolite.

3.3. Molecular modeling studies

3.3.1. Diffusion characteristics of the molecules in MFI

The MG picture shows (Fig. 7) the fitting of **3**–**5** (CPK model) inside the MFI pores (cross-section of the 10-MR). The diffusion of **5** through MFI is possible, but diffusion of **3** and **4** is not possible (Table 5). The diffusion of the molecules along the '*b*'-direction in a 10-M straight channel was carried out. The molecule passes through several energy maxima and minima, while diffusing through a unit-cell. It is observed that **5** has a diffusion energy barrier of 9.3 kcal/mol. Similar calculations for diffusion of molecules **3**, **4** and **6** were also made. The results of these calculations are given in Table 5. The diffusion energy barrier for the three isomers of nitrotoluene and dinitrotoluene increase in the order $\mathbf{5} < \mathbf{3} < \mathbf{4} < \mathbf{6}$, the calculated diffusivity being in the order $\mathbf{5} > \mathbf{3} \cong \mathbf{4}$. The mean energies of interaction of the isomers of nitrotoluene are also in the order $\mathbf{6} > \mathbf{4} \cong \mathbf{3} > \mathbf{5}$. Thus, our calculations indicate that the diffusivity of **5** in MFI is distinctly more than those of **3** and **4**. This is in conformity with the results

Table 4
Characterization of catalyst before and after reaction

Description	BET[a]	External[a]	Pore volume (cm^3/g)	Micropore volume (cm^3/g)
Fresh H-beta (formulated)	516.9	289.9	0.239	0.054
After deactivation	34.2	30.0	0.085	0.002
Fresh H-beta (non-formulated)	638.6	141.7	0.151	0.061
After deactivation	143.4	68.8	0.075	0.022

[a] Surface area (m^2/g).

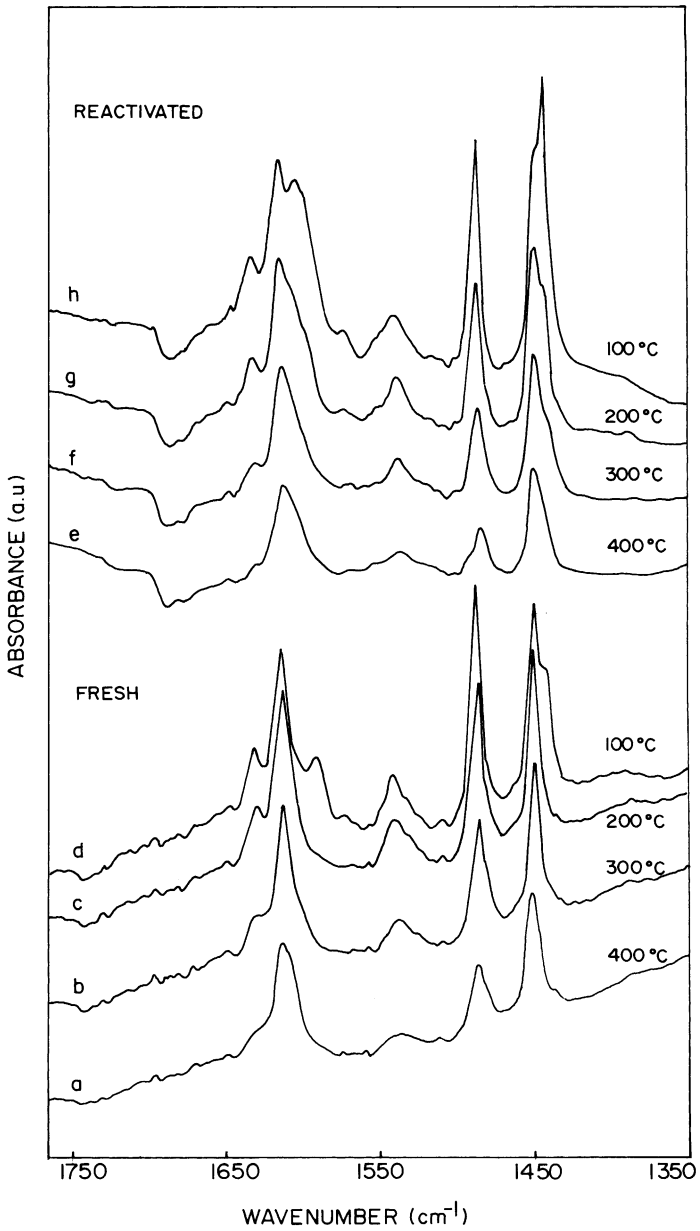

Fig. 6. (a–h) Pyridine adsorbed FTIR spectra of fresh and reactivated samples.

of an earlier calculation [18]. Our calculations based on adsorption and diffusion energy barriers inside MFI, indicate that the reactant molecules **1**–**2** are more mobile (Table 5). However, the diffusion energy barrier of **2** inside, MFI is larger than that for **1** and **5**, because of the preferred orientation of these molecules inside the zeolite pores [23]. The phenyl ring of **5** lies parallel to the diffusion plane (elliptical plane of *b*-axis) while diffusing through MFI channel [23]. The diffusion of the **5** shows two minima across the

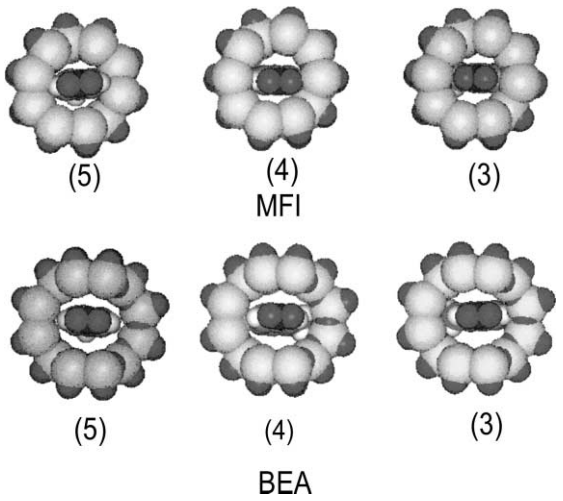

Fig. 7. The MG picture shows the fitting of **3**–**5** (CPK model) inside beta zeolite and MFI pores (cross-section of the 12- and 10-MR). Hydrogen atoms are whitish gray, carbon atoms are green, nitrogen atoms are dark blue, oxygen atoms are red and silicon atoms are yellow. Molecules **3**–**5** vary tightly fits in the pore of MFI (10-MR). In case of beta zeolite molecule **5** fits freely, whereas **4** and **3** fit more tightly in the pores even though it is 12-MR ring.

unit-cell. This happens when the phenyl ring is at the locations where the straight channels and sinusoidal channels intersect. These intersections occur twice in a unit-cell of MFI [42] and the diffusion energy profile pattern observed is in correspondence with this symmetry (not shown). Whenever the phenyl group of the molecule passes through the wall of the zeolite framework, the phenyl ring is found to be parallel to elliptical plane. Prins and co-workers [43] reported the change of coordination of aluminum from tetrahedral to octahedral would further reduce the pore diameter by ∼1 Å and this will hinder the diffusivity of *para*-isomer, affecting the shape-selectivity; these are corroborated by experimental results.

3.3.2. Diffusion characteristics of the molecules in BETA

The MG picture shows (Fig. 7) the fitting of **3**–**5** (CPK model) inside the beta pores (cross-section of the 12-MR). From the molecular fittings, it appears that the diffusion of **5** is possible through the beta zeolite pores, whereas diffusion of **3** and **4** seems to be difficult even though the pore size is larger than the size of **3** and **4**; the difficulty may arise from molecular interaction with the zeolite wall. The structure of beta can be represented as an inter-growth of two well-defined polymorph structures, both of them having three-dimensional pore architecture. The diffusion of the reactant and the three possible product molecules for the nitration reaction was carried out along the '*a*'-direction in the 12-MR channel. The diffusion was studied for five unit-cells shown in Fig. 8. Fig. 8 shows a MG picture of the minimum energy configuration of **5** inside beta. The variation in the interaction energy between **5** and beta is also included in the form of a graph. Similar calculations for diffusion of molecules **3**, **4** and **6** were also made. The salient information derived from these diffusion

Table 5
The deepest minima, peak maxima, the diffusion energy barriers, mean energy and diffusivity for organic molecules in zeolites

Zeolite	Molecule[a]	Deep minima (kcal/mol)	Peak maxima (kcal/mol)	Energy barrier (kcal/mol)	Mean energy (kcal/mol)	Diffusivity (mean/min)
MFI	**1**	−10.671	−9.183	1.488	−9.893	0.927
	2	−29.363	−6.550	22.813	−21.474	0.731
	3	−33.175	7.698	41.402	−10.227	0.303
	4	−34.448	19.287	53.735	−11.897	0.345
	5	−34.560	−25.247	9.313	−29.734	0.860
	6	−40.444	96.119	136.563	0.550	0.014
Beta	**1**	−8.819	−6.844	1.981	−07.766	0.881
	2	−19.321	−14.887	4.437	−17.010	0.880
	3	−27.948	−17.572	10.176	−23.225	0.831
	4	−28.383	−14.672	14.672	−26.613	0.838
	5	−30.975	−24.023	6.924	−27.204	0.878
	6	−28.626	−27.827	18.443	−31.530	0.807

[a] Code as in Table 2.

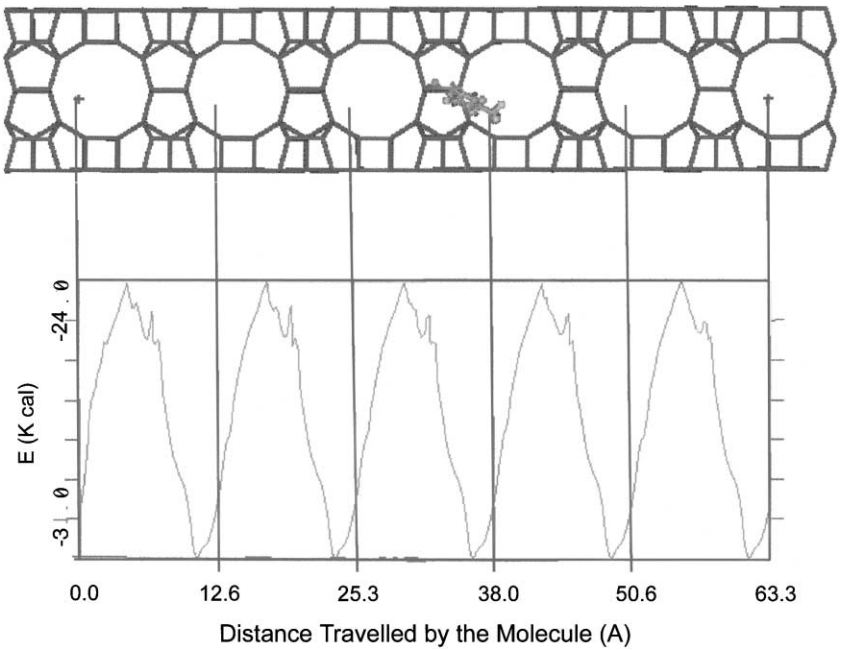

Fig. 8. Variation of the interaction energy of **5** and the beta framework as the molecule diffuses through the 12-M channel. The cross-section of the 12-M windows in the perpendicular direction in shown. A typical minimum energy configuration of the molecule during the diffusion is also included.

studies is summarized in Table 5. All of the molecules have one maxima when they diffuse through one unit-cell of beta; this maxima occurs when the molecule moves from one 12-M intersection to the other 12-M intersection. The mean energy is closer to the minimum energy values, which indicates that the molecule will diffuse selectively. Mean energy values and the diffusivity is given in Table 5. Results indicate that the diffusivity decreases in the order of **5** > **3** > **4**. The diffusion energy barrier is more for **4** as compared to the barriers for **5** and **3**. These results indicate that there will be high selectivity for the diffusion of **5** in the case of beta zeolite.

We have also analyzed the orientation of **5** when it diffuses inside the 12-MR straight channel of beta, to understand the following features: (a) the favorable and unfavorable orientations of **5** inside beta and (b) the residence time of **5** at various locations inside the straight channel of beta. In the diffusion of **5**, the phenyl ring lies parallel to the diffusion plane (elliptical plane of *b*-axis) [23]. The diffusion of the **5** shows minima across the unit-cell when the phenyl ring is at the locations where the straight channels and perpendicular channels intersect. Whenever the phenyl group of the molecule passes through the wall of the zeolite framework, the phenyl ring is found to be parallel to diffusion plane. Our results, are consistent with the hypothesis that upon adsorption of the reactant on a rigid surface such as the zeolite framework, steric hindrance would direct the orientation of the aromatic in the adsorbed state in a way that the substituent on the aromatic ring points towards the zeolite cavity where the least repulsion would be expected. During the toluene nitration Al is changing its coordination from tetrahedral to octahedral [43], reducing the pore size by ∼1 Å. Beta zeolite has three-dimensional interconnected channel system with 12-M elliptical channels having a diameter 7.6 × 6.4 Å. This will further reduce the pore size by ∼1 Å and will impart the *para*-selectivity in toluene nitration due the diffusional constraints. These results agree with experimental observations.

That the *para*-selectivity during the toluene nitration remains more or less constant even after deactivation

may be due to the partial blockage of the zeolite pores (active sites) and the remaining open pores will lead to the formation of *para*-isomer selectively.

4. Conclusion

Para-nitrotoluene is selectively formed by the vapor phase nitration of toluene using dilute nitric acid over beta zeolite at 120 °C in high yield with longer catalyst life. The catalyst is deactivated due to the deposition of oxidation products partially blocking the pores and fouling the catalyst surface. Even though the catalyst is deactivated; the selectivity for *para*-nitrotoluene is maintained because of shape-selectivity and favorable orientation of toluene molecule. One of the major advantages of this process is the use of dilute nitric acid as a nitrating agent, leading to high selectivity towards *para*-nitrotoluene and longer catalyst life. This method is superior to those using acetic anhydride or acyl nitrate as reported earlier. There is no usage of sulfuric acid, which is essential in the conventional process, thus, avoiding hazardous waste disposal, which makes the process environmentally friendly. The deactivation study reveals that the zeolite is deactivated mainly due to the partial blockage of pores during the course of the reaction and by fouling the catalyst surface by high boilers such as 4-nitrobenzoic acid (major) and anthraquinone (trace). The molecular modeling study indicates that *para*-selectivity is due to faster diffusion of *para*-isomer in the pores of the catalyst.

Acknowledgements

The author thanks CSIR, New Delhi, for financial support in the form of SRF to SBW. The authors also thank Dr. S.G. Hegde and Dr. Sourav Paul for their valuable discussion.

References

[1] K. Winnacker, L. Kuchler, in: H. Harnisch, R. Steiner, K. Winnacker (Eds.), Chemische Technologie (Band 6): Organische Technologie II, 4th Edition, Carl Hanser Verlag, Munchen, 1982, p. 169.
[2] V.P. Glusshko (Ed.), Thermodynamic Properties of Individual Substances, Vol. 1, Nauka, Moscow, 1978.
[3] Ullmann's Encyclopedia of Industrial Chemistry, VCH, Weinheim, Vol. A17, 1991, p. 411.
[4] M. McKee, R.H. Wilhelm, Ind. Eng. Chem. 28 (1936) 662.
[5] S. Suzuki, K. Tahmori, Y. Ono, Chem. Lett. 5 (1986) 747.
[6] S. Suzuki, K. Tahmori, Y. Ono, J. Mol. Catal. 43 (1987) 41.
[7] G.A. Olah, V.V. Krishnamurthy, S.C. Narang, J. Org. Chem. 47 (1982) 596.
[8] A. Cornelis, Gerstmans, P. Laszlo, Chem. Lett. 11 (1988) 1839.
[9] A. German, T. Akouz, F. Figueras, Appl. Catal. A: Gen. 136 (1996) 57.
[10] A. German, T. Akouz, F. Figueras, J. Catal. 147 (1994) 163.
[11] D. Akolekar, G. Lemay, A. Sayari, S. Kaliaguine, Res. Chem. Interm. 21 (1995) 7.
[12] S.H. Nagi, E.A. Zubkoz, V.G. Shubin, Izv. Aka. Nauk SSSR, Ser. Khim. 7 (1990) 1650.
[13] J.M. Riego, Z. Sedin, J.M. Zaldivar, N.C. Marziano, C. Toratato, Tetrahedron Lett. 37 (1996) 513.
[14] E. Suzuki, K. Tohmori, Y. Ono, Chem. Lett. 11 (1987) 2273.
[15] B.M. Choudary, M. Sateesh, M. Lakshmi Kantan, K. Koteswara Rao, K.V. Ram Prasad, K.V. Raghavan, J.A.R.P. Sharma, Chem. Commun. 1 (2000) 25–26.
[16] D. Vassena, D. Malossa, A. Kogelbauer, R. Prins, in: M.M.J. Treacy, B.K. Markus, M.E. Bisher, J.B. Higgins (Eds.), Proceedings of 12th International Zeolite Conference, Materials Research Society Warrendale, Pennsylvania, USA, 1999, p. 1909.
[17] J.M. Smith, H. Liu, D.E. Resasco, Stud. Surf. Sci. Catal. 111 (1997) 199–206.
[18] T.J. Kwok, K. Jayasuriya, J. Org. Chem. 59 (1994) 4939–4942.
[19] W.M. Meier, D.H. Olson, Ch. Baerlocher, Atlas of zeolite structure types, Zeolites, Vol. 17, Elsevier, Amsterdam, 1996, p. 1.
[20] A.T. Hagler, S. Lifson, P. Dauber, J. Am. Chem. Soc. 101 (1979) 5122.
[21] P. Dauber-Osguthorpe, V.A. Roberts, D.J. Osguthorpe, J. Wolff, M. Genest, A.T. Hagler, Proteins: structure, Function Genet. 4 (1988) 31.
[22] R.C. Deka, R. Vetrivel, J. Catal. 174 (1998) 88.
[23] S.B. Waghmode, P. Bharathi, S. Sivasanker, R. Vetrivel, Microp. Mesop. Mater. 38 (2000) 433.
[24] A. Chatterjee, R. Vetrivel, J. Chem. Soc., Faraday Trans. 91 (1995) 4313.
[25] H. van Koningsveld, H. van Bekkum, J.C. Jansen, Acta Crystallogr. B 43 (1987) 127.
[26] J.M. Newsam, M.M.J. Treacy, W.T. Koetsier, C.B. De Gruyter, Proc. R. Soc. London, Ser. A 420 (1988) 375.
[27] R. Vetrivel, C.R.A. Catlow, E.A. Colbourn, Stud. Surf. Sci. Catal. 49 (1989) 231.
[28] Y. Nakazaki, N. Goto, T. Inui, J. Catal. 136 (1992) 141.
[29] J.A. Horsley, J.D. Fellmann, E.G. Derouane, C.M. Freeman, J. Catal. 147 (1994) 231.
[30] R. Millini, S. Rossini, Stud. Surf. Sci. Catal. 105 (1996) 1389.
[31] R.C. Deka, R. Vetrivel, Chem. Commun. 21 (1996) 2397.
[32] R.C. Deka, R. Vetrivel, A. Miyamoto, Topics Catal. 9 (1999) 225.
[33] R.C. Deka, R. Vetrivel, J. Mol. Graphics Mod. 16 (1998) 157.
[34] P. Bharathi, S.B. Waghmode, S. Sivasanker, R. Vetrivel, Bull. Chem. Soc. Jpn. 72 (2161) 1999.

[35] P. Bharathi, R.C. Deka, S. Sivasanker, R. Vetrivel, Catal. Lett. 55 (1998) 113.
[36] P. Tomlinson-Tschaufeser, C.M. Freeman, Catal. Lett. 60 (1999) 77.
[37] G. Seo, H.S. Jeong, J.M. Lee, B.J. Ahn, Stud. Surf. Sci. Catal. 105B (1997) 1431.
[38] L.V. Malysheva, E.A. Paukshtis, K.G. Ione, Catal. Rev. Sci. Eng. 37 (1995) 179.
[39] B.-L. Su, V. Norberg, Zeolite 19 (1) (1997) 65–74.
[40] C. Jia, P. Massiani, D. Barthomeuf, J. Chem. Soc., Faraday Trans. 89 (19) (1993) 3659–3665.
[41] B.C. Lippens, J.H. de Boer, J. Catal. 4 (1965) 319.
[42] H. Van Koningsveld, J.C. Jansen, H. van Bekkum, Zeolites 10 (1990) 235.
[43] M. Haouas, A. Kogelbauer, R. Prins, Catal. Today 70 (2000) 61–65.